Revised *CONBUILDMAT-D-19-09093*

1 Effect of seawater on early age hydration, microstructure and

2 mechanical properties of cement paste

3 Peiran Li[a], Wengui Li[a*], Tao Yu[b], Fulin Qu[a], Vivian W.Y. Tam[c]

4 [a] School of Civil & Environmental Engineering, University of Technology Sydney, NSW 2007, Australia

5 [b] Department of Civil and Environmental Engineering, The Hong Kong Polytechnic University, Hong Kong, China

6 [c] School of Computing, Engineering and Mathematics, Western Sydney University, NSW 2751, Australia

7 **Abstract**: Using seawater for concrete manufacturing promisingly provides significant economical

8 and environmental benefits. In this study, ordinary Portland cement (OPC) hydration in distilled

9 water and seawater and compares the evolution of solid phases was investigated by heat evolution,

10 hydrated phase, hydration kinetics, and microstructure characterization. The results show that

11 seawater can promote the early hydration of tricalcium silicate (C_3S) during the hydration

12 acceleration period. The hydrated phase assemblage was influenced by the dissolved ions in seawater.

13 Friedel's salt was detected as a specific hydration phase in seawater, which was formed by chemical

14 combination between the aluminate ferrite monosulfate (AFm) phase and chloride ions. In addition,

15 the monocarboaluminate can be converted into a stable phase as Friedel's salt in the seawater, due to

16 the reaction with chloride ions. Furthermore, the ettringite becomes more stable when coexists with

17 Friedel's salt than that with monocarboaluminate, and thus ettringite formed in seawater remains

18 67% higher than that formed in distilled water at the later curing age. Moreover, additional

19 unhydrated cement and less amorphous calcium silicate hydrate (C-S-H) were formed in seawater,

20 which might be responsible for the slightly lower compressive strength of cement mortar prepared by

21 seawater. Generally, a modeled evolution of the solid phase and pore solution have been established,

*Corresponding author: School of Civil and Environmental Engineering, University of Technology Sydney, NSW 2007, Australia

Email address: wengui.li@uts.edu.au (Wengui Li)

22 which agrees well with the characteristics of the dissolution of mineral phase, precipitation of

23 hydration products and changes of pore solution. The related results can provide an insight into the

24 applications of seawater and sea sand concrete for infrastructures.

25 **Keywords**: Seawater; Cement hydration; Chloride ion; Mechanical strength; Microstructure

26 # 1. Introduction

27 The rapid development in urbanization and industrialization causes a heavy demand for new concrete

28 infrastructures such as buildings, bridges, pavements, and ports, etc. [1]. Due to low cost and high

29 durability requirements, concrete has become the most commonly used material of about 30 billion

30 tons used annually [2]. However, concrete manufacturing is always accompanied by huge carbon

31 emissions and results in harmful effects on the environment [3, 4]. In addition, large concrete demands

32 lead to considerable consumption of the sand, clay, rock, and water, which severely threaten the

33 ecology of the land, water resources, and air quality. In other words, concrete manufacturing inevitably

34 causes a significant impact on the environment, such as contamination of groundwater and soil,

35 riverbed erosion and biodiversity deterioration. Thus, it is essential to develop sustainable concrete

36 with both economic and ecological benefits [5-13].

37 Applications of seawater and sea sand in concrete is a promising option for easing resources crisis

38 and construction cost, especially in the coastal and island regions. However, due to the excess chloride

39 in seawater and sea sand, issues should be firstly solved on the aspect of physico-mechanical

40 performance, durability reduction and rebar corrosion [14]. Investigations found that concrete using

41 seawater can cause a 20% reduction in initial slump flow and a nearly 30% loss in initial setting time,

42 compared with the freshwater-made concrete at the same water to bind ratio [15, 16]. In addition, using

43   seawater increases the early concrete strength by about 10 to 25% within 14 days, and makes limited

44   influences on the later age strength [15-19]; the drying shrinkage of concrete made by seawater is

45   approximately 15% lower than that of concrete with fresh water [20]. These property changes are

46   mainly attributed to the introduced ions, such as sodium, magnesium and sulfate, etc, and the high

47   concentration of chloride would significantly affect the cement hydration. It has been proposed that

48   two main reasons are responsible for the stimulated hydration by chloride. Firstly, calcium hydroxide

49   (CH) would react with calcium chloride ($CaCl_2$) to form insoluble solid phase calcium oxychloride

50   (CAOXY) when seawater is used as mixing water mixed with cement [21], as illustrated in Eq. (1).

51   During the reaction process, chloride reduces the concentration of alkalinity and calcium in solution,

52   which promotes the dissolution of cement particles for improving the hydration rate. Secondly,

53   chloride can react with aluminates and ferrites [22, 23], forming insoluble phase as

54    $3CaO \cdot Al_2O_3 \cdot CaCl_2 \cdot 10H_2O$, (or if iron presents, $3CaO \cdot Al_2O_3 \cdot Fe_2O_3 \cdot CaCl_2 \cdot 10H_2O$), as described in

55   Eq. (2). The phase has been named as Friedel's salt [24], which belongs to the family of hydrated

56   calcium aluminate phase (AFm phase) [25]. This group of compounds is formed as a lamellar

57   structure related to $M(OH)_6$ octahedral ions based on brucite-like layers, and become charged by

58   one-third of divalent cations replaced by trivalent cation (e.g. aluminum and iron). As a result, the

59   charged AFm phase attracts positive ions such as sulfate, carbonate, and chloride. The general

60   formula of these compounds can be described as $[Ca_2(Al, Fe)(OH)_6] \cdot X \cdot xH_2O$, where X represents

61   the attracted monovalent anion or half of divalent anion bound [26-29]. Friedel's salt is beneficial to

62   densify the cement matrix [30], and can convert mutually with monosulfate by changing the

63   concentration of sulfate and chloride ions [31]. Most studies have found that using seawater seems

64   not to introduce serious defects in concrete structure, but can improve physical and mechanical

65   properties such as density, compressive strength and elastic modulus [15,17,32-34]. The

66   contradictories are bascially the strength developments at later curing age in concrete with seawater,

67   such as an one-year superiority of compressive strength in concrete with seawater [16], a 13% lower

68   28-day compressive strength [35] or the comparable strength [15, 36]. Furthermore, concerns still

69   remain due to the issue of rebar corrosion and undetermined durability by chloride ions.

70    $$CaCl_2 + 3Ca(OH)_2 + 12H_2O \Rightarrow 3Ca(OH)_2 \cdot CaCl_2 \cdot 12H_2O \qquad (1)$$

71    $$C_3A + 2NaCl + Ca(OH)_2 + 10H_2O \Rightarrow C_3A \cdot CaCl_2 \cdot 10H_2O + 2Na^+ + 2(OH)^- \qquad (2)$$
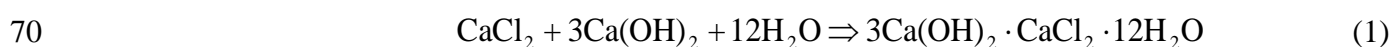
72   Therefore, further studies are imperative to fundamentally investigate the properties of cement

73   composites with seawater as mixing water including hydration mechanism, mechanical properties

74   and druability. The aim of this study is to investigate the effect of seawater on the cement hydration

75   and microstructure development, and to establish a correlation with the mechanical properties for

76   Portland cement. This study applied the modern characterization methods to investigate the heat

77   evolution of hydration, phase assemblages, kinetics, morphology, microstructure developmemnt and

78   compressive and flextural strengths of cement paste with seawater, and conmpared the results with

79   the ones mixed with distilled water. The measured and calculated changes of phase compositions are

80   compared for the evolution of the effect of seawater on cement hydration and delivered an extensive

81   experimental investigations on the effect of seawater in cement martor. The related results will

82   provide an insight into the prospect of seawater concete design and application for concrete

83   infrasctures with special consideration of mitigating the chloride induced steel reinforcement

84   corrosion.

2. Experimental program

2.1 **Raw materials**

The cement used in the study was the OPC conforming to Australian standard AS 3972 (General purpose and blended cements). The oxide compositions of the cement measured by X-ray fluorescence (XRF) were summarized in Table 1. The contents of limestone and gypsum were provided by the cement supplier. After the XRF data was corrected by deducing the chemical composition of the two given minerals, the approximate mineral composition in OPC was obtained through Bogue calculation [38]. The minieral composition and physical properties are shown in Table 2. Two types of mixing water: (1) distilled water (D-water); and (2) natural seawater (S-water), were applied. The natural seawater was obtained from the Congwong Beach of Sydney coast in Australia. Table 3 shows the chemical composition of D-water determined by inductively coupled plasma mass spectrometry (ICP-MS), which is close to the world average concentrations of ions in surface seawater [39]. Natural river sand (R-sand) and washed sea sand (S-sand) are used in cement mortars, which contains few impurities such as clay and sea salt. The particle sizes distribution of the used R-sand and S-sand are shown in Fig. 1.

2.2 Experimental methods

2.2.1 Heat of hydration

To investigate the effect of seawater on the hydration of OPC, an isothermal heat conduction calorimeter (TAM Air) was applied to measure the heat of hydration during the first 60 hrs. D-water and S-water were used as mixing water in samples. The water to binder (w/b) ratios of the samples are 0.5 and 0.7. Firstly, 30.00 g cement was weighed and mixed with weighted D-water or S-water

106   for 60 sec, followed by being injected into ampoules through a syringe. Afterward, the ampoules

107   loaded with samples and those with references were capped and lowered into the calorimeter

108   simultaneously. Due to the external premixing procedure, very early cement hydration cannot be

109   measured from calorimeter, and the signal of heat flow became stable after approximately 60 mins.

110   In order to reduce the experimental error, the references applied dry sand (quartz) and distilled water

111   to respectively simulate the OPC and the certain water used in samples, with the same total heat

112   capacity. The composition of the samples with S-water and D-water were summarized in Table 4.

113   The samples were denoted by their "water type + w/b ratio". For example, the "D-0.5" represented

114   OPC with D-water at a w/b ratio of 0.5. The final exotherms were corrected by subtracting the

115   baseline obtained before and after the measuring process.

116   2.2.2 Phase and micromorphology

117   Semi-quantitative X-ray diffraction (XRD), Thermogravimetry/Differential scanning calorimetry

118   (TG/DSC) and Scanning electron microscope-Energy dispersive X-ray spectroscopy (SEM-EDS)

119   were adopted to analyze the phase evolution during cement hydration in D-water and S-water. The

120   samples were OPC pastes with D-water or S-water at w/b ratio of 0.5. The pastes were prepared in a

121   Hobart mixer and cast in seated plastic molds at the size of 50 mm $\times$ 50 mm $\times$ 50 mm, then cured in a

122   standard curing chamber with a temperature of 20 °C and 95% relative humidity. After 1 day of

123   hydration, the samples were demolded and further cured at the previous condition. Afterward, the

124   samples with different hydration ages were dried by two different treatments. For those hydrated less

125   than 1 day, the samples were transferred into a vacuum freeze dryer to remove free water after

126   reaching the specified ages; the drying process lasted for 2 days at -55 °C in vacuumed condition.

127   For those hydrated longer than 1 day, the hardened cement pastes were crushed into small pieces and

128   the debris from the inside part of paste were collected, followed by being immersed into isopropanol

129   for the hydration stoppage. In this way, the ongoing hydration process can be terminated. After

130   immersed for 7 days, the debris was transferred and stored in a desiccator over silica gel for 3 days.

131   Furthermore, some debris was ground to pass through a sieve with a screen aperture of 75 μm, as the

132   powder samples applied to TG and XRD measurement.

133   In terms of TG/DSC analysis, the equipment STA449 F5 JUPITER was used to determine caloric

134   effects and mass changes in the temperature-rise period. About 30 mg of dried powder sample was

135   loaded into an alumina crucible, purged with nitrogen and heated from 25 °C to 1000 °C with the

136   temperature increasing rate of 10 °C/min. With the increase of temperature, the decomposition of

137   hydration products can be determined by mass loss from chemically bound water and carbonate, and

138   thus the content of the corresponding hydrate phase can be determined. In addition, the endothermic

139   peaks exhibited in DSC curves illustrated the enthalpies of transitions from decompositions of phase.

140   As a result, the area of the endothermic peak can be converted into the value of enthalpy of transition,

141   which helps determine the certain reaction, molar content of involved substance, and solid

142   composition. Furthermore, some moist samples as contrast groups were also measured which were

143   not terminated hydration, ground and dried before, to determine the content of pore solution.

144   X-ray diffraction analysis was conducted by Bruker D8 Discover with the diffraction angle (2θ)

145   ranged from 5° to 70° and the scan step size of 0.02°. Cu K(alpha) radiation (k = 1.54056 A°) was

146   used as the X-ray source. Before measurement, the powder samples were blended with 10% titanium

147   oxide as the special ingredients of the internal standard method. Semiquantitative analysis of mineral

148 solid phases was conducted through the peak heights and peak areas of the intensity of corresponding

149 phases. Micromorphology analysis was conducted by applying the scanning electron microscope

150 (SEM) Zeiss Supra 55vp combining with energy dispersive X-ray spectrometry (SEM-EDS).

151 2.2.3 Mechanical strength

152 Cement mortars were prepared for compressive strength measurements according to ASTM C109

153 (Standard Test Method for Compressive Strength of Hydraulic Cement Mortars). For each group,

154 three cubic specimens (50 mm $\times$ 50 mm $\times$ 50 mm) were prepared. The mix design of cement mortar

155 was listed in Table 5. All specimens were cured for 1 day in the chamber before demolded and

156 further cured in standard curing chamber (temperature of 25 °C and relative humidity of 95%). The

157 cement mortars were tested at diffeent curing ages of 7, 14 and 28 days for compression test. The

158 compression machine of UH500 was applied with a loading rate of 0.1 mm/min in stroke. Cement

159 mortars were prepared for flexural strength measurements. For each group, three prismatic

160 specimens (40 mm $\times$40 mm $\times$160 mm) were prepared. The curing condition and tested ages are as

161 same as those for compressive strength. The flexural strength test in accordance with ASTM C348-18

162 (Standard Test Method for Flexural Strength of Hydraulic-Cement Mortars). The cement mortars were

163 tested at different curing ages of 7, 14 and 28 days.

164 **3. Results and discussions**

165 **3.1 Heat evolution of hydration**

166 Hydration heat evolution of OPC was measured with w/b ratios of 0.5 and 0.7 hydrated in D-water

167 and S-water, respectively. The exotherm of OPC in 60 hrs was shown in Fig. 2(a). The ordinates of

168 the figure, normalized heat/heat flow, are the quantifiable exothermic units released per gram of

169   cement. At the early age of the hydration process, the period exhibiting insignificant heat flow was

170   the induction period, which was caused by the restricted precipitation and the extremely slow rate of

171   dissolution of cement [40-43]. It was observed that the duration of the induction period of hydration

172   in D-0.5 and S-0.5 ranged from 1.54 to 1.56 hrs. Furthermore, increasing the w/b ratios from 0.5 to

173   0.7 had a limited impact on the period of induction. It reveals that the dissolved ions in S-water do

174   not have a great influence on the initial dissolution and precipitation process, although there might be

175   a new solid phase formed. The initial hydration still subjected to the limited surface with low

176   interfacial energy, which is consistent with the dissolution theory based on a geochemical approach

177   to crystal dissolution [44, 45].

178   In the acceleration period, it was observed that the duration to reach the hydration peak (Peak I)

179   was greatly reduced by 36% for the OPC paste with S-water, in comparison to the OPC with D-water.

180   Furthermore, the exotherm peak of paste in S-water exhibited 44% higher than that with D-water.

181   Hence, it demonstrates that the dissolved ions in S-water can significantly promote cement hydration.

182   According to the previous studies [21, 22], chloride was the dominator that can chemically bind with

183   calcium, aluminate, and ferrite ions to form insoluble phases such as calcium oxychloride and

184   Friedel's salt. The involved chloride ions contribute to promoting the precipitation of the dissolved

185   mineral ions in solution. Thus, according to the chemical equilibrium, the dissolution rate of

186   unhydrated clinkers is promoted. The stimulating effect is a particular significance to the main mineral

187   tricalcium silicate (C_3S) [46].

188   When the heat flow started to decrease, an exotherm with acromion presented from around 10 to

189   15 hrs or later. The acromion was a part of another peak (Peak II), which was overlapped with Peak I.

190   The Peak II was formed from the heat of hydration of calcium aluminate (C_3A) and calcium

191   aluminoferrite (C_4AF) [28]. During this hydration period, the concentration of sulfate in solution

192   decreased over time since the gypsum has completely depleted before C_3A and C_4AF. Ettringite,

193   therefore, became less stable with a lower sulfate solution and subsequently started to convert into

194   the AFm phase [47]. In S-water, however, the hydration rate increased during this period, which was

195   greatly affected by the various dissolved ions, especially under the condition with a high

196   concentration of chloride. During the period, it was found from the following analysis of TG and

197   XRD that Friedel's salt was intensively formed after gypsum was completely consumed. Thus, the

198   formation of Friedel's salt promoted the hydration of aluminate and ferrite minerals. Furthermore, an

199   extension of acromion appeared in samples at a high w/b ratio of 0.7, in which the mass diffusion

200   and transformation were less restricted than the samples at a low w/b ratio. For the OPC with S-water

201   at the w/b ratio of 0.7, more ions from seawater were involved in cement hydration, and thus the

202   acceleration effect of hydration can be further improved, in comparison to the counterpart at w/b

203   ratio of 0.5.

204   In Fig. 2(b), the accumulated heat evolution shows that the gap of hydration heat released from

205   S-0.5 and S-0.7 started to widen after 5 hrs, and S-0.7 released nearly 20% additional heat after 60

206   hrs. As for D-0.5 and D-0.7, however, the two exotherms showed a limited difference, releasing less

207   heat than those in S-water. It indicates that the dissolved ions in S-water can promote hydration,

208   especially chloride which accounted for more than half of the ions in S-water. The following

209   conclusions can be drawn through the comparison: the hydration rate of C_3S is greatly affected by

210   the concentration of chloride in solution, which is correlated with the equilibrium concentration of

211 CAOXY. If the involved chloride is increased but the concentration of chloride in mixing water is

212 not changed, such as of S-0.5 and S-0.7, the hydration rate of C_3S will not be obviously accelerated.

213 Unlike C_3S, the hydration of aluminate and ferrite can be stimulated with the increasing content of

214 chloride involved, which is due to the further formation of Friedel's salt.

215 **3.2** Thermogravimetric and X-ray diffraction analysis

216 The compositions of OPC paste with D-water and S-water were determined by TG/DSC and XRD

217 analysis. Fig. 3 shows the TG and the derivative thermogravimetry (DTG) results of OPC paste in

218 D-water at various hydration times. The peaks of mass loss displayed in DTG curves indicate that the

219 precipitation of ettringite and dissolution of gypsum took place earlier even in 1 hr of hydration. The

220 other hydrated phases, such as C-S-H and portlandite, had hardly formed yet during the initial

221 hydration period, which resulted in the DTG curves exhibited closer to zero significantly. After 8 hrs

222 of hydration, it was observed that portlandite and C-S-H had formed and constituted the main part of

223 the hydrated phase, indicating the hydration reaction of C_3S happened rapidly during this period. The

224 rapid reaction was consistent with the aforementioned characteristic of heat release in the

225 acceleration period.

226 After 12 hrs hydration, gypsum was completely dissolved and depleted. Due to the decreasing

227 concentration of sulfate in the pore solution, the preformed ettringite had become unstable and

228 gradually converted to the AFm-formed phase at a slow rate [48]. In DTG curves, it was found that

229 the sample with a 12 hrs hydration had the largest peak at around 100 °C, compared to the samples

230 with other lengths of hydration time. The peak indicated a maximum mass loss, which attributed to

231 the dehydration of ettringite, water desorption and water loss from C-S-H gel layers. As an

232   amorphous solid phase, the dehydration reaction of C-S-H occurred continuously from 105 °C to

233   1000 °C [49], and the amount of dehydrated water increased with the increasing temperature. In Fig.

234   3, it was observed that the mass loss increased with the increasing hydration age, especially from 200

235   to 400 °C, which illustrated an increasing content of C-S-H with ongoing hydration.

236   The decomposition of portlandite took place at approximately 420 °C, followed by the

237   decomposition of the carbonate phase at the temperature over 600 °C. As the main production of

238   OPC, the content of CH and C-S-H increased with the hydration degree, and their growth rates

239   gradually decreased at the later age. After 28-day hydration, the content of CH and C-S-H was nearly

240   constant and hardly increased. Monocarboaluminate (carbo-AFm), instead of monosulfoaluminate

241   (sulfo-AFm), was detected as the final hydration product of the residual aluminate phase, due to the

242   excess of carbonate ions provided from limestone [50, 51]. Calcite is the major mineral phase of

243   limestone added in OPC cement, which was found slightly decreased during the ongoing hydration

244   period. The other type of carbonate, magnesite, was found increased at the later age, which

245   decomposed at around 600 °C [52]

246   The aforementioned TG analysis can be further confirmed by XRD analysis. Fig. 4 gives the

247   representative diffraction patterns for the OPC paste with D-water. It was observed that the amounts

248   of the four main OPC minerals decreased at different rates. Due to the high solubility, C_3A and

249   gypsum reacted rapidly to form ettringite which can be detected after 2 hrs of hydration. The

250   hydration properties of C_4AF was similar to that of C_3A, but the rate was much slower. When

251   gypsum was completely depleted after 12 hrs of hydration, the XRD showed no sulfo-AFm phase

252   (characteristic peak 2-Theta at 9.895°) during the following hydration period. Instead, the content of

253   carbo-AFm (characteristic peak 2-Theta at 11.670°) was found increasing along with hydration. In

254   terms of silicate minerals, a great amount of C_3S was found dissolved in the first 2 days of hydration,

255   and the further hydration rate gradually decreased with the hydration time. After 63 days, the extent

256   of hydration of C_3S was observed nearly unchanged in hardened OPC paste. For another OPC

257   mineral, the C_2S hydrated much slower, attributed to the less solubility than that of C_3S. It could be

258   found that some of the C_2S remained unhydrated after 63 days of hydration.

259   In Fig. 5, the cement paste with S-water shows a higher weight loss within 7 days than that of

260   paste with D-water, which reveals the enhanced early hydration of OPC paste in S-water, due to the

261   influences by salt ions such as sodium, sulfate, and especially chloride ions. As mentioned above, the

262   presence of chloride could accelerate the precipitation of calcium ions, which was beneficial to the

263   dissolution of minerals. In terms of the sulfate ions involved in hydration, 0.034 molar of sulfate

264   could be supplied from the 5.84 wt.% of gypsum in 100 g of OPC, and 0.0014 molar of sulfate was

265   introduced from S-water, which accounts for only 4% of that from gypsum. However, despite the

266   small variation of sulfate content, Fig. 5 reveals a similar or less amount of ettringite formed in the

267   S-water after 1 hr and 2 hrs of cement hydration. This is probably due to the formation of calcium

268   oxychloride [21], which occupies the limited surface of cement particles and restricts the formation

269   of ettringite [40]. As a result, the generation of ettringite was slightly retarded at the initial stage of

270   cement hydration.

271   The formation of Friedel's salt was the most significant difference between pastes with D-water

272   and S-water. The Friedel's salt could be dehydrated at 120 °C [53], and thus cannot be distinguished

273   with carbo-AFm from TG analysis. In the X-ray patterns of cement paste with S-water, the

274 characteristic peak (2-Theta at 11.192°) confirmed the presence of Friedel's salt as shown in Fig. 6.

275 In particular, the hydration products carbo-AFm was never formed in cement paste with S-water,

276 which was quite different from cement paste with D-water. The results suggest that carbo-AFm was

277 instable with chloride ions and could be converted into Friedel's salt in seawater. Also, it was feasible

278 to bind chloride ions by increasing the content of the AFm phase in OPC. Furthermore, it should be

279 noted that more carbonate was observed decomposed over 600 °C in cement paste with S-water,

280 which was due to the formed magnesite from the excess carbonate from the decomposition of

281 carbo-AFm and the additional magnesium introduced from S-water.

282 **3.3 Modeling of hydration**

283 The evolution of the solid phase and pore solution was investigated by applying the quantitative

284 analysis of TG/DSC results and semiquantitative analysis of XRD patterns. The peak areas in the

285 DSC curve represented the enthalpy change, which reflected the energy transfer from a certain

286 reaction of decomposition [54], to support the quantitative analysis from mass loss. Taking samples of

287 cement paste with D-water in 2 hrs and cement paste with S-water in 12 hrs, as shown in Fig 7, the

288 corresponding hydration phase could be quantified through methods combining TG and DSC. Based

289 on these data, a linear regression was used to investigate the correlation between the TG and DSC.

290 Fig. 8 demonstrates a reasonable agreement and close values to the linear relation for evaluating

291 gypsum, portlandite, and calcite. Therefore, the data from DSC confirmed the TG results, which could

292 be the supplementation and correction in the estimation of the solid phase. The extent of OPC

293 hydration was evaluated based on the changes in the peak intensity of the crystalline phase in XRD

294 patterns. The peak intensity was corrected by the intensity of TiO_2, which was the calibration

295 substance.

296 According to the result, a modeled evolution was set up regarding the various phases from OPC

297 hydration in D-water and S-water as a function to the hydration time as shown in Figs. 9 and 10. It

298 was observed that a small amount of gypsum dissolved in the first 1.5 hrs, along with the hydration

299 of C_3A minerals, and a small amount of ettringite was found precipitated. After 8 hrs of hydration, it

300 was noted that 35% of C_3S dissolved in S-water, which was 16% more than that in D-water,

301 conformed to the aforementioned greater heat released from the hydration in S-water during this

302 period. After 7 days of hydration, the total amount of hydrated C_3S in D-water was nearly catch up

303 with that of paste in S-water. At the later age of 63 days, the C_3S minerals were almost completely

304 hydrated in D-water. However, 8% C_3S was detected remaining unhydrated in S-water, showing that

305 S-water might decrease the later-age hydration rate of OPC. Furthermore, the total content of C-S-H

306 in S-water was lower, although it was beneficial to form C-S-H rapidly in the early 7 to 15 days of

307 hydration. Overall, the results showed that the amount of C-S-H decreased by nearly 10 wt.% in

308 S-water after 63 days of hydration. The decreases might be due to the increasing proportion of other

309 hydration products such as ettringite and Friedel's salt, which led to a less negative effect on the later

310 age strength of OPC.

311 The gypsum in D-water and S-water was completely disappeared after 12 hrs hydration. At this

312 moment, the content of ettringite was no longer increased but started to convert to the AFm phase.

313 For the cement paste with D-water, the content of ettringite accounted for 12.7% of the total mass

314 and then decreased to 6.6% after 63 days. With the presence of limestone in OPC, nearly 48%

315 ettringite was converted to the carbo-AFm phase instead of sulfo-AFm after 63 days, since carbonate

316   could replace sulfate ions from AFm to form the stable phase [50, 51]. In comparison, ettringite in

317   S-water increased by 7% compared to that in D-water after 18 hrs. However, only 22% of ettringite

318   had decomposed after 63 days, indicating that the ettringite exhibited more stable in S-water. The

319   reason is that the introduced chloride ions in S-water are more stable to combine the AFm phase than

320   carbonate from limestone. Therefore, the formation of sulfo-AFm became more difficult, which

321   resulted in more uncombined sulfate ions presented in pore solution to hinder the decomposition of

322   ettringite.

323   The hydration ratio of C_3A and C_4AF shows no significant discrepancy in D-water and S-water.

324   Fig. 9 shows that C_3A and C_4AF were hydrated completely in 4 and 7 days, respectively. As for C_2S,

325   only a similar 53% of this mineral phase was hydrated after 63 days in both D-water and S-water,

326   although S-water can accelerate the hydration of C_2S by 5% in the first 3 days. The formation of

327   Friedel's salt can be detected after 1 day of hydration in cement paste with S-water, which gradually

328   increased to nearly 7% of the total mass after 7 days and then kept unchanged in the further 56 days.

329   Friedel's is formed mainly from the residual unhydrated aluminate phase and chloride after ettringite.

330   The result showed that ettringite formed early than Friedel's salt, which can be due to the higher

331   stability and insolubility of ettringite than Friedel's salt [31, 53,55]. In other words, Friedel's salt

332   cannot be formed when gypsum exists because only ettringite precipitates during this period, which

333   was confirmed by the evolution of the solid phase from experimental results, as shown in Fig. 9. It

334   means that ettringite does not have the chloride-binding capacity in the concentration of seawater.

335   The point can also be drawn that if aluminate or ferrite minerals were used for binding chloride to

336   reduce chloride concentration in cement, adding gypsum would weaken the binding effect.

337　　Compare to the solid phase from hydration in D-water, it was observed that no carbo-AFm formed

338　in S-water. The significant differences revealed that the chloride in S-water can convert carbo-AFm

339　to Friedel's salt by replacing carbonate ions, to form Friedel's salt which was more stable than

340　carbo-AFm. Furthermore, the study found no carbo-AFm formed throughout the hydration of 63

341　days, which illustrated that the involved chloride became beyond the binding capacity of aluminate

342　and ferrite phase in OPC. Due to the replacement effect of carbonate in AFm, the S-water paste

343　remained 1.5% more calcite and 2.3% more magnesite than those of D-water paste. The consumption

344　volume of pore solution can represent the extent of hydration [56], from the reaction of free water

345　converting into chemically combined water and hydroxyl. Throughout the entire hydration process,

346　the amount of pore solution in S-water was always lower than that of D-water, particularly from 2

347　hrs to 15 days of hydration. The rapid consumption in S-water can inevitably influence the early

348　strength and workability and may affect construction efficiency [15].

349　**3.4 Microstructural characterization**

350　The scanning electron microscopy (SEM) was conducted to morphologically describe the

351　microstructure of the cement pastes with D-water and S-water in Fig. 11. After 12 hrs hydration, it

352　could be observed that the C_3S particles in D-water remained very smooth, with only a small number

353　of C-S-H nucleus attached in the surface of C_3S particles, as shown in Fig. 11(a). For the cement

354　paste with S-water, however, the finer C-S-H nucleus precipitated intensively on the surface of C_3S

355　particles in Fig. 11(b), conformed to the accelerating effect in S-water on early hydration. After 2

356　days of hydration, the hydration product of C-S-H, portlandite, and ettringite could be observed in

357　OPC paste. The solid phase in D-water paste distributed randomly at the initial age of hydration, and

358 mutually overlapped and connected the nearby solid particles, as shown in Fig. 11(c). Due to the

359 rapid hydration in S-water paste, a denser microstructure formed can be observed in Fig. 11(d),

360 revealing the previous scattered phase has connected and converted to the plate-like forms. The rapid

361 formation of the denser microstructure indicated S-water is beneficial to early strength.

362   The elemental mapping of S-water paste after 4 days of hydration was displayed in Fig. 12, which

363 was conducted by energy-dispersive X-ray spectrometry. By comparing the morphology of certain

364 hydration products and the elemental composition, the formed hydration phases can be identified. It

365 was found brucite or brucite-like layers hydrotalcite (Mg(Al, Fe) xH_2O) in S-water paste from the

366 hydration phase of magnesium [57]. Along with the interface between the hydrated phase of calcium

367 and aluminate, Friedel's salt can be identified with a higher content of chloride. The Friedel's salt

368 previously crystallized as flat hexagonal platelets [53] and subsequently stacked as a thicker form. In

369 addition to the chloride binding capacity of the AFm phase, it showed that the chloride could be

370 physically absorbed by C-S-H gels [58], which resulted in a wide distribution of chloride in cement

371 paste.

372 **3.5 Mechancial strength**

373 The compressive strength of mortars prepared by D-water and S-water was investigated as illustrated

374 in Fig. 13. It was found that S-water increased the early compressive strength of cement mortar at 7

375 days by nearly 15% in both specimens with river sand and sea sand, compared with those with

376 D-water. As for the later curing age, however, the compressive strength of the cement mortar with

377 D-water increased considerably than those with S-water. Although the specimens with S-water had

378 higher compressive strength at 14 days, they were subsequently exceeded by their counterparts with

379 D-water after 28 days. It conformed to the promoted early hydration and the slightly retarded

380 hydration of C_3S in S-water, which is the primary mineral phase in OPC contributing to compressive

381 strength. In addition, river sand was better than sea sand regarding the growth of compressive

382 strength, as a better grading distribution in river sand can obtain a denser structure. By contrast, the

383 particle size distribution in sea sand is relatively concentrated, reducing the filling effect. Its smooth

384 surface, furthermore, weakens the bound properties between cement and aggregates, thus gaining a

385 relatively lower compressive strength. The difference between specimens with seawater and distilled

386 water is less than 8% in flexural strength, as shown in Fig. 14. However, using sea sand reduces the

387 flexural strength by nearly 25% from 7 days to 28 days, indicating that the ions in seawater present

388 less impact but the flexural strength is greatly decreased by the poor particle size distribution of the

389 aggregate.

390 ## 4. Conclusions

391 In this study, the hydration properties of OPC in D-water and S-water have been investigated by

392 analyzing the heat evolution, hydrated phase, hydration kinetics, and microstructures. The main

393 conclusions can be drawn up as follows:

394 (1) The hydration of OPC can be accelerated by S-water, which is mainly due to the chloride

395   promoting the precipitation of calcium, aluminate, and ferrite. The accelerated hydration rate

396   indicates the positive effect of S-water, especially in the stage of 2 to 48 hrs. The formation of

397   Friedel's salt led to the accelerated hydration of C_3A and C_4AF, and therefore the hydration rates

398   of the two minerals were increased at high w/b ratios, with additional chloride involved in

399   hydration.

400   (2) The hydration rate of C_3S is greatly promoted in seawater especially at the early age of 1 day due

401   to the involved chloride in hydration. At the same ion concentrations, the hydration rate of C_3S is

402   not significantly increased by mixing with more seawater. However, the hydration of aluminate

403   and ferrite can be stimulated with the increasing amount of seawater involved, which may be due

404   to the formation of Friedel's salt.

405   (3) Affected by the rapid hydration in S-water, the early compressive strength of OPC mortar

406   increased rapidly. For the cement mortar with S-water at the w/b ratio of 0.4, the compressive

407   strength of 7 days and 14 days increased by 15% and 5%, respectively compared to those of

408   counterparts with D-water. However, the compressive strength of 28 days is nearly the same as

409   that of specimens with D-water. Seawater can influence the flexural strength of less than 8%

410   from 7 days to 28 days while using sea sand instead of river sand can decrease flexural strength

411   by 25% due to the poor particle size distribution.

412   (4) The chloride in S-water promoted the early hydration reaction and influenced the hydrate

413   assemblage of the hydrating cement paste. In the presence of chloride, Friedel's salt was more

414   stable than carbo-AFm in OPC paste. Due to chemical equilibrium, the decomposition rate of

415   ettringite at 63 days was reduced from 51% to 22%, and more carbonate was formed, such as

416   magnesite from 2.3% to 4.6% of the total mass. As a result, the chloride binding capacity of

417   OPC could be weakened by sulfate from gypsum, for that gypsum can react with aluminate to

418   form stable phase ettringite, which has no chloride-binding capacity.

419   (5) It was found that in the later age of 28 days, 8% C_3S remains unhydrated in OPC paste with

420   S-water, and the mass of C-S-H is 10% lower than that of OPC paste with D-water. The decrease

421 in mass might be due to the increasing proportion of other hydration products, such as ettringite

422 and Friedel's salt, and thus had a less negative effect on the later strength of OPC.

Declaration of Competing Interest

424 The authors declare that they have no known competing financial interests or personal relationships

425 that could have appeared to influence the work reported in this paper.

Acknowledgments

References

434 [1] W. F. Laurance, A. Peletier-Jellema, B. Geenen, et al., M.W. Doyle, D.G. Havlick, Reducing the
435   global environmental impacts of rapid infrastructure expansion, Curr. Biol. 25(7) (2015) 259-262.

436 [2] P.J. Monteiro, S.A. Miller, A. Horvath, Towards sustainable concrete, Nat. Mater. 16(7) (2017)
437   698.

438 [3] V. Malhotra, Making concrete" greener" with fly ash, Concr. Int. 21(5) (1999) 61-66.

439 [4] P. Mehta, Concrete technology for sustainable development - an overview of essential elements,
440   Concrete Technology for a Sustainable Development in the 21st Century 83 (1999).

441 [5] A. Torres, J. Brandt, K. Lear, J. Liu, A looming tragedy of the sand commons, Sci. 357(6355)
442   (2017) 970-971.

443 [6] P.K. Mehta, Greening of the concrete industry for sustainable development, Concr. Int. 24(7)
444   (2002) 23-28.

445 [7] P.K. Mehta, Global concrete industry sustainability, Concr. Int. 31(2) (2009) 45-48.

446 [8] K.P. Mehta, Reducing the environmental impact of concrete, Concr. Int. 23(10) (2001) 61-66.

447 [9] Z. Tang, Y. Hu, V.W.Y. Tam, W. Li, Uniaxial compressive behaviors of fly ash/slag-based
448   geopolymeric concrete with recycled aggregates, Cem. Concr. Compos. 104 (2019) 103375.

449 [10] S.D.C. Gomes, J.L. Zhou, W. Li, G. Long. Progress in manufacture and properties of construction
450   materials incorporating water treatment sludge: A review, Resour. Conserv. Recy. 145 (2019)
451   148-159.

452 [11] Z. Luo, W. Li, V.W.Y. Tam, J. Xiao, S.P. Shah. Current progress on nanotechnology application
453   in recycled aggregate concrete, J Sustainable Cem-Based Mater. 8 (2) (2019) 79-96.

454 [12] S.A. Miller, A. Horvath, P.J. Monteiro, Impacts of booming concrete production on water
455   resources worldwide, Nat. Sustain. 1(1) (2018) 69.

456 [13] W. Dong, W. Li, Z. Tao, K. Wang, Piezoresistive properties of cement-based sensors: review and
457   perspective, Constr. Build. Mater 203 (2019) 146-163.

458 [14] Ş. Erdoğdu, T. Bremner, I. Kondratova, Accelerated testing of plain and epoxy-coated
459   reinforcement in simulated seawater and chloride solutions, Cem. Concr. Res. 31(6) (2001)
460   861-867.

461 [15] A. Younis, U. Ebead, P. Suraneni, A. Nanni, Fresh and hardened properties of seawater-mixed
462   concrete, Constr. Build. Mater 190 (2018) 276-286.

463 [16] H.Y. Ghorab, M. Hilal, A. Antar, Effect of mixing and curing waters on the behaviour of cement
464   pastes and concrete Part 2: Properties of cement paste and concrete, Cem. Concr. Res. 20(1)
465   (1990) 69-72.

466 [17] O.E.Gjørv, Ø.Vennesland. Diffusion of chloride ions from seawater into concrete. Cem. Concr.
467   Res. 9(2) (1979) 229-238.

468 [18] W. Chalee, C. Jaturapitakkul, P. Chindaprasirt. Predicting the chloride penetration of fly ash
469   concrete in seawater. Mar. Struct. 22(3) (2009) 341-353.

470 [19] .T. Nishida, N. Otsuki, H. Ohara, Z.M. Garba-Say, T. Nagata, Some considerations for
471   applicability of seawater as mixing water in concrete, J Mater. Civ. Eng. 27(7) (2013) 4014004.

472 [20] K. Katano, N. Takeda, Y. Ishizeki, K. Iriya, Properties and application of concrete made with sea

473   water and un-washed sea sand, Proceedings of Third International conference on Sustainable

474   Construction Materials and Technologies, Kyoto, 2013.

475   [21] Y. Farnam, S. Dick, A. Wiese, J. Davis, D. Bentz, J. Weiss, The influence of calcium chloride

476   deicing salt on phase changes and damage development in cementitious materials, Cem. Concr.

477   Compos. 64 (2015) 1-15.

478   [22] A.M. Rosenberg, Study of the mechanism through which calcium chloride accelerates the set of

479   portland cement, ACI Journal Proceedings, 61(10) (1964) 1261-1270.

480   [23] M. Thomas, R. Hooton, A. Scott, H. Zibara, The effect of supplementary cementitious materials

481   on chloride binding in hardened cement paste, Cem. Concr. Res. 42(1) (2012) 1-7.

482   [24] P. Friedel, Sur un chloro-aluminate de calcium hydraté se maclant par compression, Bulletin Soc.

483   Franc. Minéral 19 (1897) 122-136.

484   [25] T. Matschei, B. Lothenbach, F. Glasser, The AFm phase in Portland cement, Cem. Concr. Res.

485   37(2) (2007) 118-130.

486   [26] D. Damidot, F. Glasser, Thermodynamic investigation of the $CaO\text{-}Al_2O_3\text{-}CaSO_4\text{-}H_2O$ system at

487   50 °C and 85 °C, Cem. Concr. Res. 22(6) (1992) 1179-1191.

488   [27] D. Damidot, S. Stronach, A. Kindness, M. Atkins, F. Glasser, Thermodynamic investigation of the

489     $CaO\text{-}Al_2O_3\text{-}CaCO_3\text{-}H_2O$ closed system at 25 °C and the influence of Na_2O, Cem. Concr. Res.

490   24(3) (1994) 563-572.

491   [28] B. Clark, P. Brown, The formation of calcium sulfoaluminate hydrate compounds: Part I, Cem.

492   Concr. Res. 29(12) (1999) 1943-1948.

493   [29] Z. Shi, M.R. Geiker, B. Lothenbach, K. De Weerdt, S.F. Garzón, K. Enemark-Rasmussen, J.

494   Skibsted, Friedel's salt profiles from thermogravimetric analysis and thermodynamic modelling of

495   Portland cement-based mortars exposed to sodium chloride solution, Cem. Concr. Compos. 78

496   (2017) 73-83.

497   [30] H. Li, N. Farzadnia, C. Shi, The role of seawater in interaction of slag and silica fume with cement

498   in low water-to-binder ratio pastes at the early age of hydration, Constr. Build. Mater. 185 (2018)

499   508-518.

500   [31] H. Hirao, K. Yamada, H. Takahashi, H. Zibara, Chloride binding of cement estimated by binding

501 isotherms of hydrates, J. Adv. Concr. Technol. 3(1) (2005) 77-84.

502 [32]M. Etxeberria, A. Gonzalez-Corominas, P. Pardo, Influence of seawater and blast furnace cement

503 employment on recycled aggregate concretes' properties, Constr. Build. Mater 115 (2016)

504 496-505.

505 [33]Y. Li, X. Zhao, R.S. Raman, Mechanical properties of seawater and sea sand concrete-filled FRP

506 tubes in artificial seawater, Constr. Build. Mater 191 (2018) 977-993.

507 [34]M. Etxeberria, J.M. Fernandez, J. Limeira, Secondary aggregates and seawater employment for

508 sustainable concrete dyke blocks production: Case study, Constr. Build. Mater 113 (2016)

509 586-595.

510 [35]S. Kaushik, S. Islam, Suitability of sea water for mixing structural concrete exposed to a marine

511 environment, Cem. Concr. Compos. 17(3) (1995) 177-185.

512 [36]Q. Li, H. Geng, Y. Huang, Z. Shui, Chloride resistance of concrete with metakaolin addition and

513 seawater mixing: A comparative study, Constr. Build. Mater. 101(1) (2015) 184-192.

514 [37]B. Lothenbach, M Zajac, Application of thermodynamic modelling to hydrated cements. Cem.

515 Concr. Res. 123 (2019) 105779.

516 [38]R.H. Bogue, The chemistry of Portland cement, New York, Reinhold Pub. Corp., 1955.

517 [39]A. Vollpracht, B. Lothenbach, R. Snellings, J. Haufe. The pore solution of blended cements: a

518 review. Mater. Struct. 49 (2016) 3341-3367.

519 [40]M.M. Costoya Fernández, Effect of particle size on the hydration kinetics and microstructural

520 development of tricalcium silicate, Lausanne, EPFL, 2008.

521 [41]D. Damidot, A. Nonat, P. Barret. Kinetics of tricalcium silicate hydration in diluted suspensions

522 by microcalorimetric measurements, J Am. Ceram. Soc. 73(11) (1990) 3319-3322.

523 [42]P. Fierens, J. Verhaegen, Hydration of tricalcium silicate in paste-kinetics of calcium ions

524 dissolution in the aqueous phase, Cem. Concr. Res. 6(3) (1976) 337-342.

525 [43]I. Odler, H. Dörr, Early hydration of tricalcium silicate II. The induction period, Cem. Concr. Res.

526 9(3) (1979) 277-284.

527 [44]P. Juilland, E. Gallucci, R. Flatt, K. Scrivener, Dissolution theory applied to the induction period

528 in alite hydration, Cem. Concr. Res. 40(6) (2010) 831-844.

529   [45] A. Kumar, S. Bishnoi, K.L. Scrivener, Modelling early age hydration kinetics of alite, Cem.
530   Concr. Res. 42(7) (2012) 903-918.

531   [46] F. Caruso, S. Mantellato, M. Palacios, R. J. Flatt, ICP-OES method for the characterization of
532   cement pore solutions and their modification by polycarboxylate-based superplasticizers, Cem.
533   Concr. Res. 91 (2017) 52-60.

534   [47] L. Black, C. Breen, J. Yarwood, C.-S. Deng, J. Phipps, G. Maitland, Hydration of tricalcium
535   aluminate (C_3A) in the presence and absence of gypsum-studied by Raman spectroscopy and
536   X-ray diffraction, J. Mater. Chem. 16(13) (2006) 1263-1272.

537   [48] B. Lothenbach, F. Winnefeld, Thermodynamic modelling of the hydration of Portland cement,
538   Cem. Concr. Res. 36(2) (2006) 209-226.

539   [49] G. Khoury, C. Majorana, F. Pesavento, B. Schrefler, Modelling of heated concrete, Mag. Concr.
540   Res. 54(2) (2002) 77-101.

541   [50] B. Lothenbach, G. Le Saout, E. Gallucci, K. Scrivener, Influence of limestone on the hydration of
542   Portland cements, Cem. Concr. Res. 38(6) (2008) 848-860.

543   [51] V. Bonavetti, V. Rahhal, E. Irassar, Studies on the carboaluminate formation in limestone
544   filler-blended cements, Cem. Concr. Res. 31(6) (2001) 853-859.

545   [52] Y. Kocak, S. Nas, The effect of using fly ash on the strength and hydration characteristics of
546   blended cements, Constr. Build. Mater. 73 (2014) 25-32.

547   [53] U. Birnin-Yauri, F. Glasser, Friedel's salt, $Ca_2Al(OH)_6(Cl, OH) \cdot 2H_2O$: its solid solutions and
548   their role in chloride binding, Cem. Concr. Res. 28(12) (1998) 1713-1723.

549   [54] Y. Kong, J. Hay, The enthalpy of fusion and degree of crystallinity of polymers as measured by
550   DSC, Eur. Polym. J. 39(8) (2003) 1721-1727.

551   [55] F. Winnefeld, B. Lothenbach. Hydration of calcium sulfoaluminate cements - Experimental
552   findings and thermodynamic modelling. Cem. Concr. Res. 40(8) (2010) 1239-1247.

553   [56] T. C. Powers, Structure and physical properties of hardened portland cement paste, J Am. Ceram.
554   Soc. 41 (1) (1958) 1-6.

555   [57] J.M. Fernández, M.A. Ulibarri, F.M. Labajos, V. Rives, The effect of iron on the crystalline
556   phases formed upon thermal decomposition of Mg-Al-Fe hydrotalcites, J. Mater. Chem. 8(11)

557   (1998) 2507-2514.

558   [58]Z. Shi, M.R. Geiker, K. De Weerdt, T.A. Østnor, B. Lothenbach, F. Winnefeld, J. Skibsted, Role

559   of calcium on chloride binding in hydrated Portland cement-metakaolin-limestone blends, Cem.

560   Concr. Res. 95 (2017) 205-216.

561

562 **List of Tables**

568

569

570

571

572

573

574 <div align="center">Table 1 Chemical composition of the OPC (oxide composites)</div>

Chemical	CaO	SiO_2	Al_2O_3	Fe_2O_3	MgO	SO_3	Na_2O	K_2O	CO_2	MnO	P_2O_5	LOI*
Component (wt.%)	62.9	20.3	4.5	4.6	1.2	2.6	0.3	0.3	2.0	—	—	4.0

575   Note: LOI* presents loss on ignition

576

577

578

579

580

581

582   Table 2 Mineral composition of Portland cement and its physical properties

Minerals	C_3S	C_2S	C_3A	C_4AF	Limestone	Gypsum
Content (wt.%)	47.16	22.72	4.14	14.00	4.54	5.59

583   Note: Specific gravity is 2800-3200; bulk density is 1200-1600kg/m^3 and average particle size (d_{50}) is 8 μm.

584

585

586

587

588

589

590 Table 3 Major chemical composition of seawater from Sydney Congwong Beach

Dissolved ions	Na^+	K^+	Ca^{2+}	Mg^{2+}	Cl^-	SO_4^{2-}
Concentration (mol/l)	0.47	0.01	0.01	0.05	0.54	0.03

591

592

593

594

595

596   Table 4 Mix design of cement paste for hydration heat analysis

| Index | W/b ratio | Sample (g) | | | Control sample (g) | | | Total heat capacity |
		OPC	D-water	S-water	Sand (Quartz)	D-water	S-water	(J/K·g)
D-0.5	0.5	9.40	4.70	—	9.40	4.70	—	26.70
S-0.5	0.5	9.40	—	4.70	9.40	—	4.70	26.70
D-0.7	0.7	7.40	5.17	—	7.40	5.17	—	27.17
S-0.7	0.7	7.40	—	5.17	7.40	—	5.17	27.17

597

598

599

600

601

602

603

Table 5 Mix design of cement mortar

Mix	Cement (kg/m^3)	D-water (kg/m^3)	S-water (kg/m^3)	R-sand (kg/m^3)	S-sand (kg/m^3)
DR*	800	320	—	1600	—
DS*	800	320	—	—	1600
SR*	800	—	320	1600	—
SS*	800	—	320	—	1600

604 Note: DR* presents the mortars prepared by D-water and R-sand; DS* represents the mortars prepared by D-water and S-sand; SR* is

605 the mortars prepared by S-water and R-sand; SS* means the mortars prepared by S-water and S-sand.

606

607

List of Figures

608

609   Fig. 1. Particle size distribution of S-sand and R-sand

610   Fig. 2. Heat evolution of OPC hydrated in D-water and S-water at w/b ratios of 0.5 and 0.7

611   Fig. 3. TG/DTG curves of OPC in D-water after 1, 2, 8, 12, 18 hr, and 1, 2, 7, 28, 63 days of

612   hydration at w/b ratio of 0.5

613   Fig. 4. XRD pattern of OPC in D-water after 2, 8 hr, and 2, 28, 63 days of hydration at w/b ratio of

614   0.5 (A –C_3S, B –C_2S, C –calcite, E –ettringite, G –gypsum, P –portlandite, M –magnesite, M_C

615   –monocarboaluminate, C_A –C_3A, C_F –C_4AF, Ti –titanium oxide for calibration reference)

616   Fig. 5. TG/DTG curves of OPC in S-water; after 1, 2, 8, 12, 18 hr, and 1, 2, 7, 28, 63 days of

617   hydration at w/b ratio of 0.5

618   Fig. 6. XRD pattern of OPC in S-water after 2, 8 hr, and 2, 28, 63 days of hydration at w/b ratio of

619   0.5 (A –C_3S, B –C_2S, C –calcite, E –ettringite, F –Friedel's salt, G –gypsum, P –portlandite, M

620   –magnesite, C_A –C_3A, C_F –C_4AF, Ti –titanium oxide for calibration reference)

621   Fig. 7. Quantitative analysis of TG/DSC in OPC hydrated in D-water and S-water

622   Fig. 8. Fitting regression of the data from TG and DSC evaluation methods of gypsum, portlandite

623   and calcite

624   Fig. 9. Evolution of solid phases model and pore solution of OPC in D-water and S-water

625   Fig. 10. Phase evolution model of OPC hydrated in D-water and S-water

626   Fig. 11. Microstructure of OPC paste hydrated in D-water and S-water in 12 hr and 2 days

627   Fig. 12. Elemental mapping of microstructures of OPC paste hydrated in S-water for 4 days

628   Fig. 13. Compressive strength of cement mortar with different types of water and sand

629

630

631

632

633

634
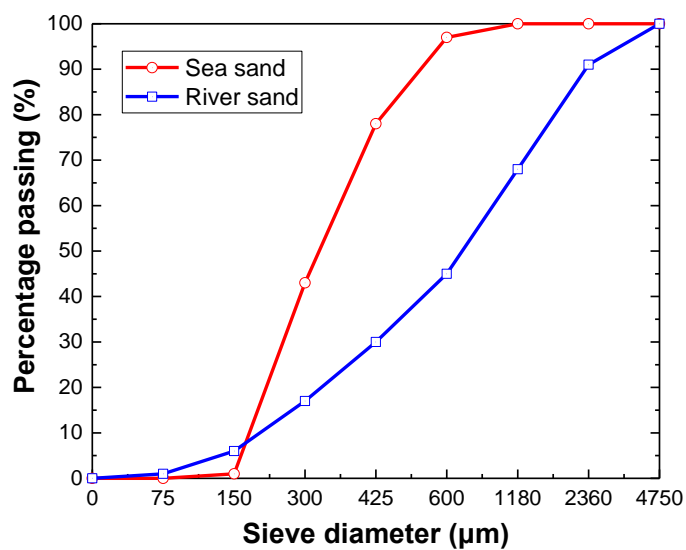
Fig. 1. Particle size distribution of S-sand and R-sand

635

636

637

638
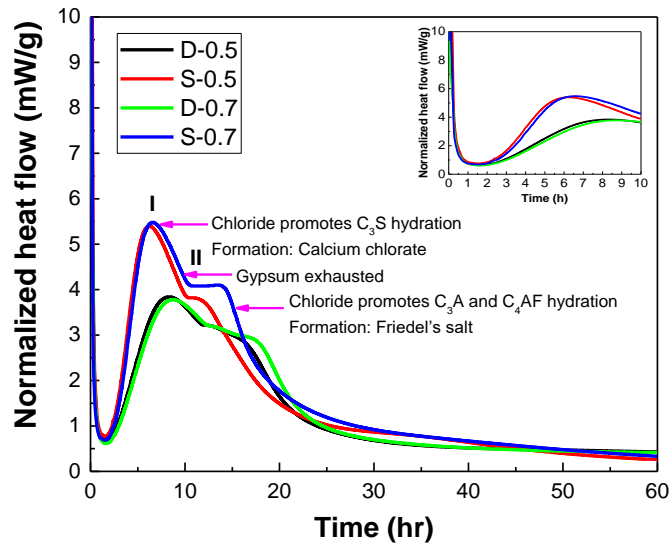
(a) Exothermic rate at w/b ratios of 0.5 and 0.7
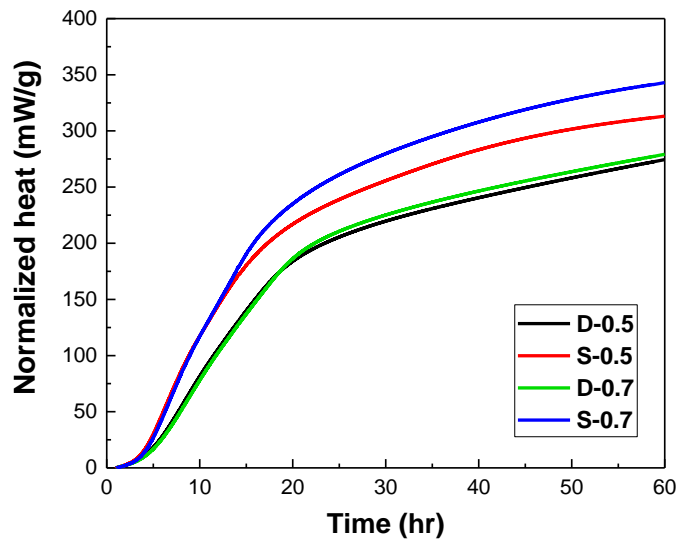
(b) Cumulative heat of hydration at w/b ratios of 0.5 and 0.7

Fig. 2. Heat evolution of OPC hydrated in D-water and S-water at w/b ratios of 0.5 and 0.7

639

640

641

642

643

644

645
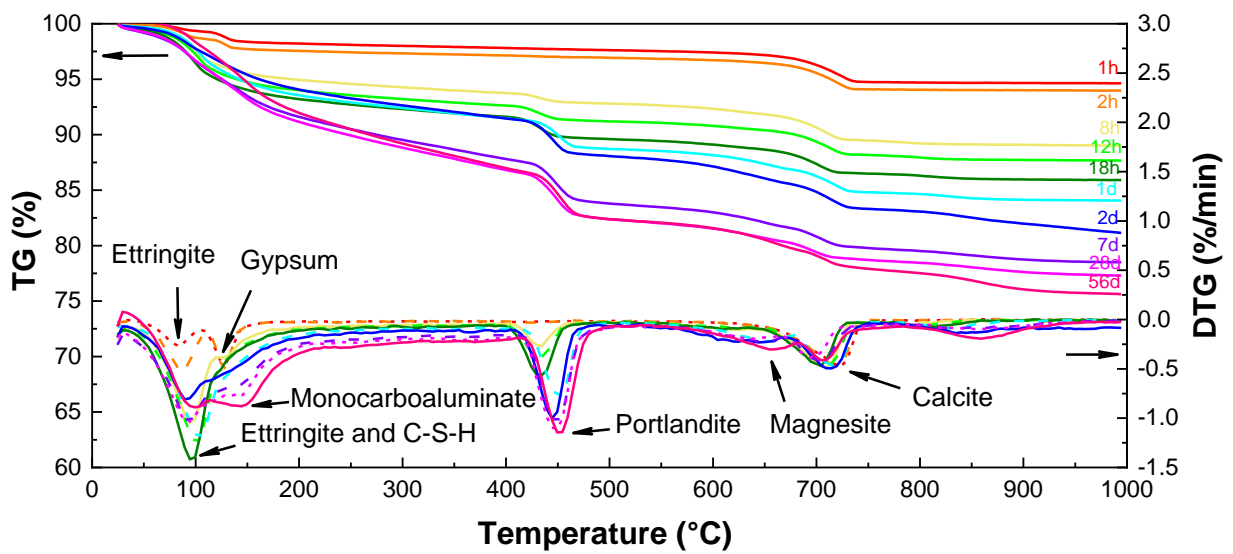
Fig. 3. TG/DTG curves of OPC in D-water after 1, 2, 8, 12, 18 hrs, and 1, 2, 7, 28, 63 days of

hydration at w/b ratio of 0.5

646

647

648

649

650

651

652
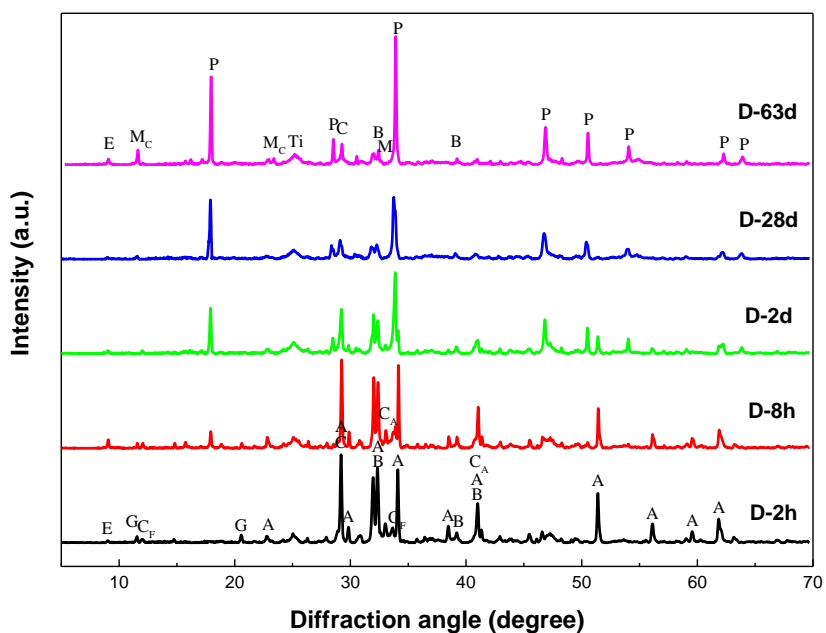
Fig. 4. XRD pattern of OPC in D-water after 2, 8 hr, and 2, 28, 63 days of hydration at w/b ratio of 0.5 (A –C_3S, B –C_2S, C –calcite, E –ettringite, G –gypsum, P –portlandite, M –magnesite, M_C –monocarboaluminate, C_A –C_3A, C_F –C_4AF, Ti –titanium oxide for calibration reference)

653

654

655

656

657

658
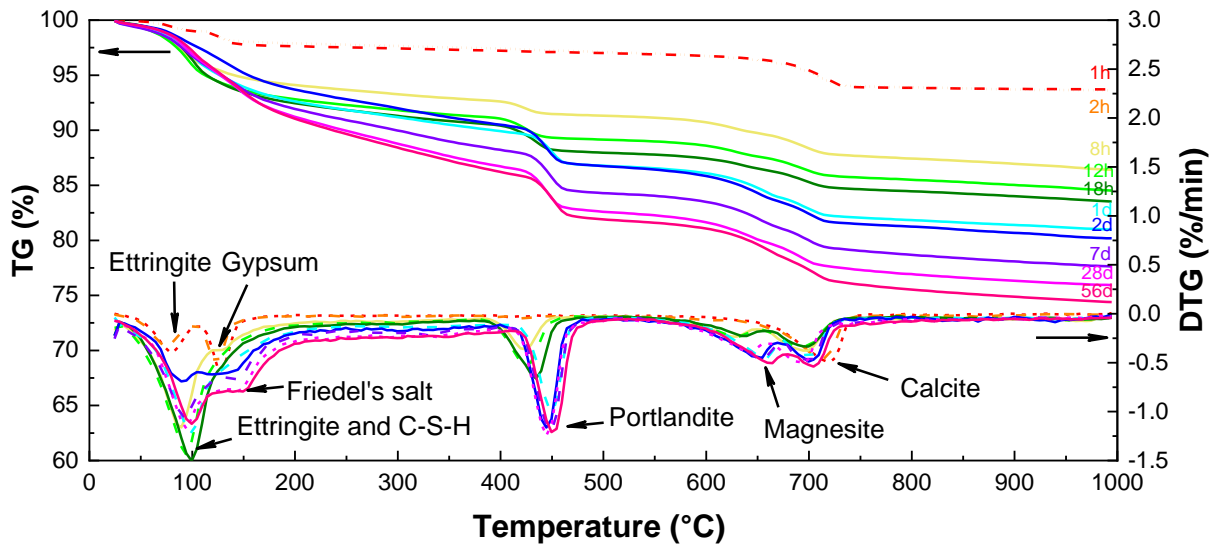
Fig. 5. TG/DTG curves of OPC in S-water; after 1, 2, 8, 12, 18 hr, and 1, 2, 7, 28, 63 days of

hydration at w/b ratio of 0.5

659

660

661

662

663

664
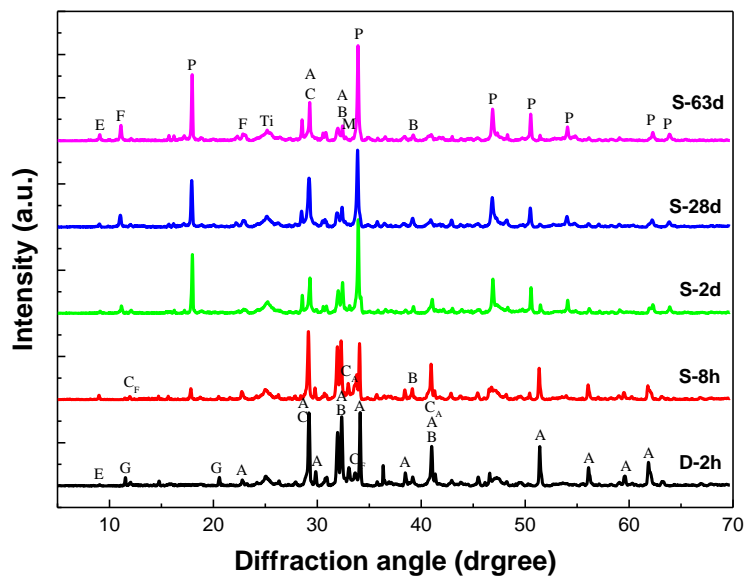
Fig. 6. XRD pattern of OPC in S-water after 2, 8 hr, and 2, 28, 63 days of hydration at w/b ratio of

0.5 (A –C$_3$S, B –C$_2$S, C –calcite, E –ettringite, F –Friedel's salt, G –gypsum, P –portlandite, M

–magnesite, C$_A$ –C$_3$A, C$_F$ –C$_4$AF, Ti –titanium oxide for calibration reference)

665

666

667

668
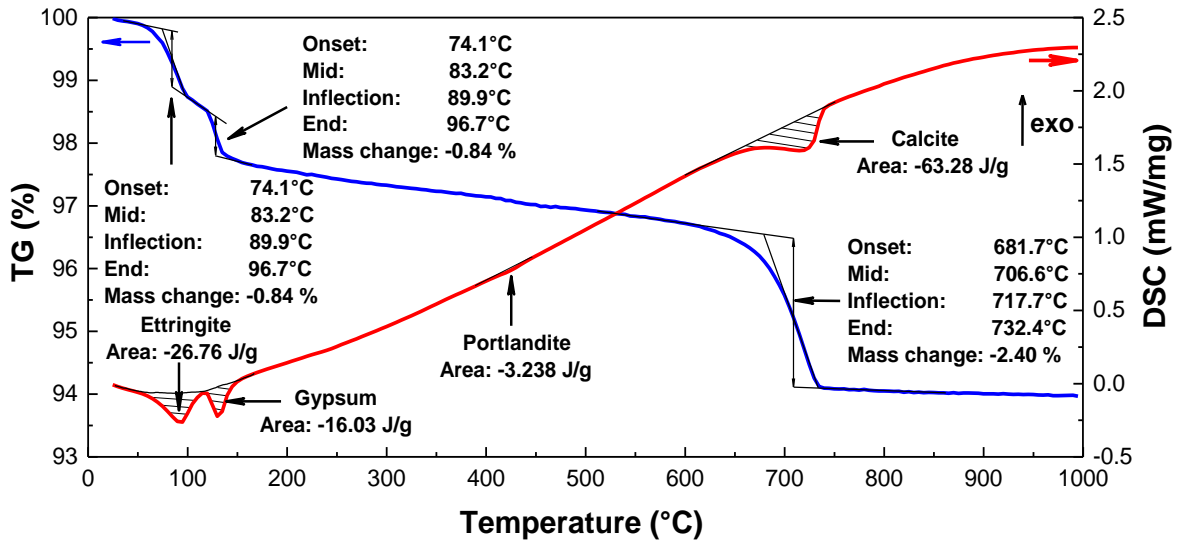
(a) TG/DSC analysis of OPC hydrated in D-water for 2 hr
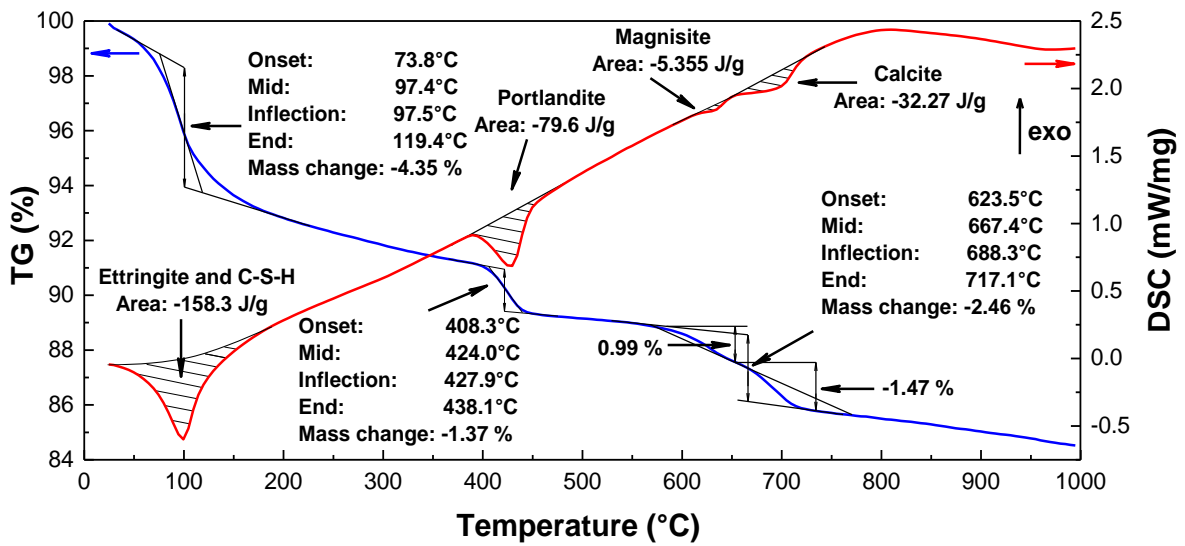
(b) TG/DSC analysis of OPC hydrated in S-water for 12 hr

Fig. 7. Quantitative analysis of TG/DSC in OPC hydrated in D-water and S-water

669

670

671

672

673

674
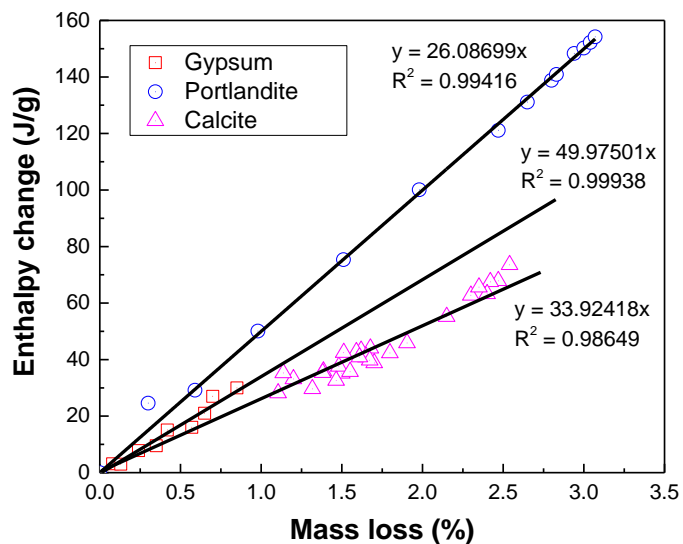
Fig. 8. Fitting regression of the data from TG and DSC evaluation methods of gypsum, portlandite

and calcite

675

676

677

678

679
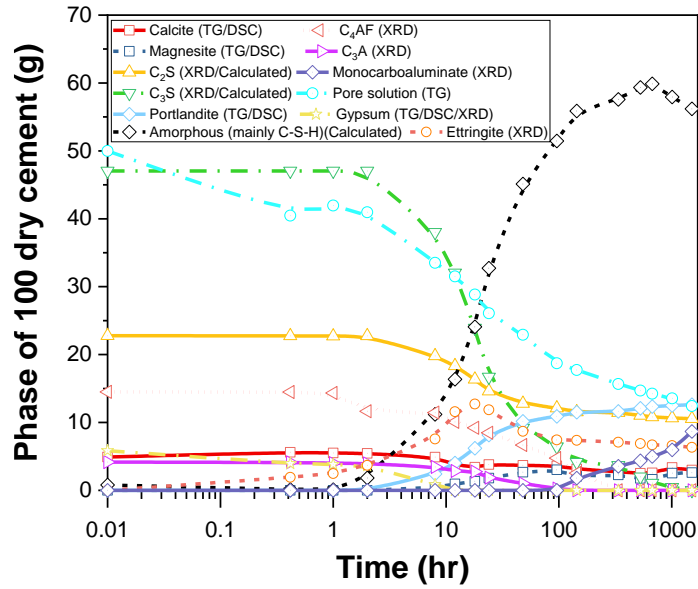
(a) OPC hydrated in D-water
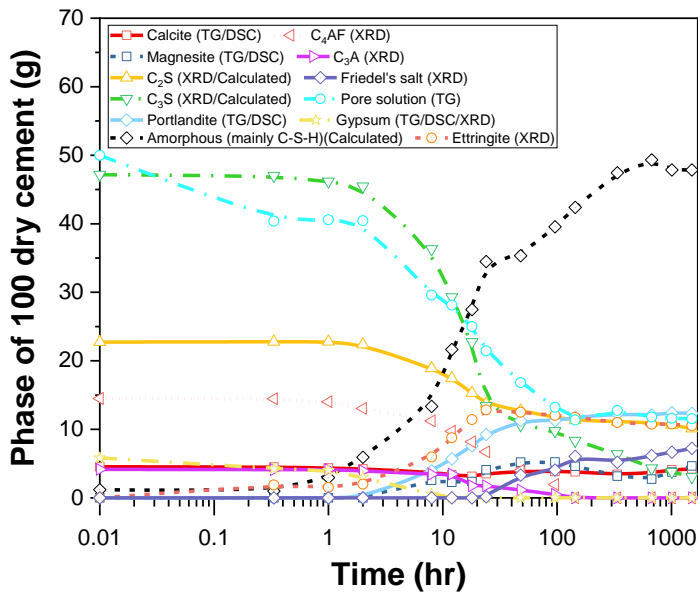
(b) OPC hydrated in S-water

Fig. 9. Evolution of solid phases model and pore solution of OPC in D-water and S-water

680

681

682
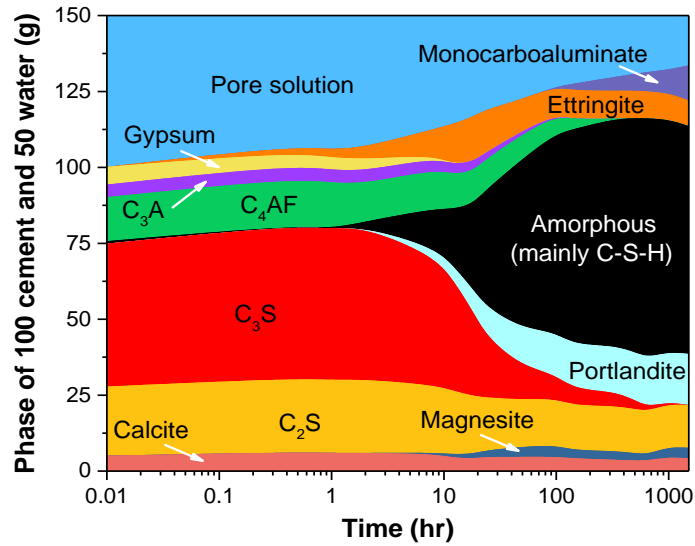
(a) OPC hydrated in D-water
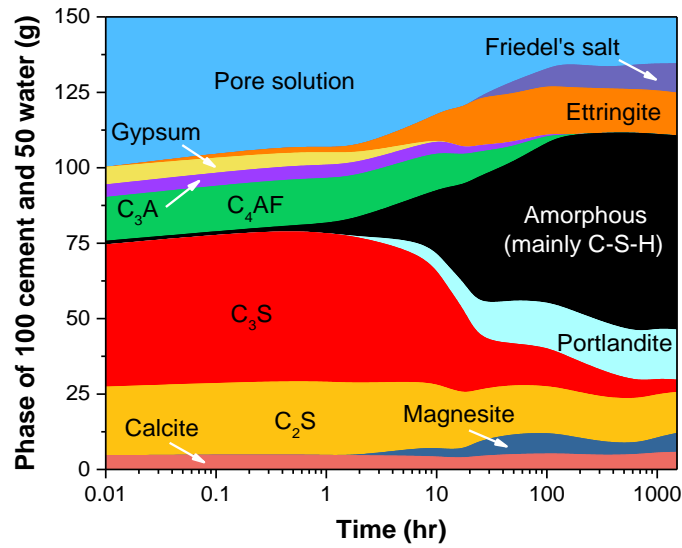
(b) OPC hydrated in S-water

Fig. 10. Phase evolution model of OPC hydrated in D-water and S-water

683

684

685

686

687
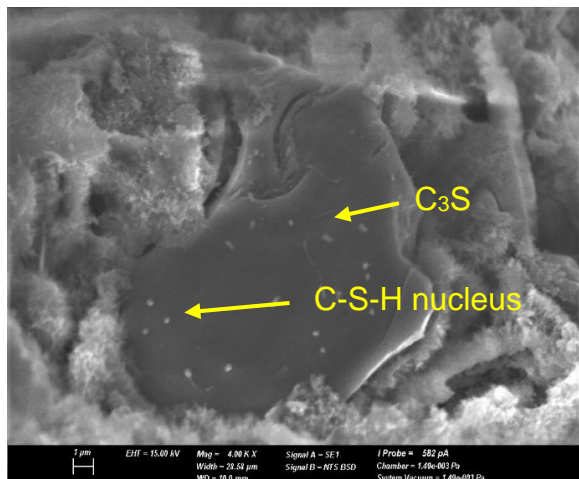
(a) OPC paste hydrated in D-water in 12 hr
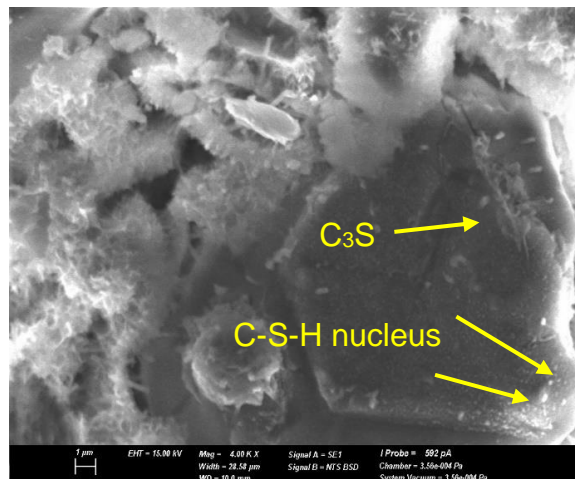
(b) OPC paste hydrated in S-water in 12 hr
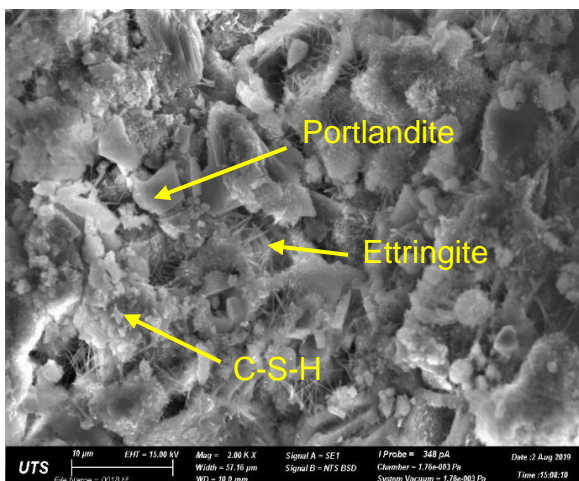
(c) OPC paste hydrated in D-water in 2 days
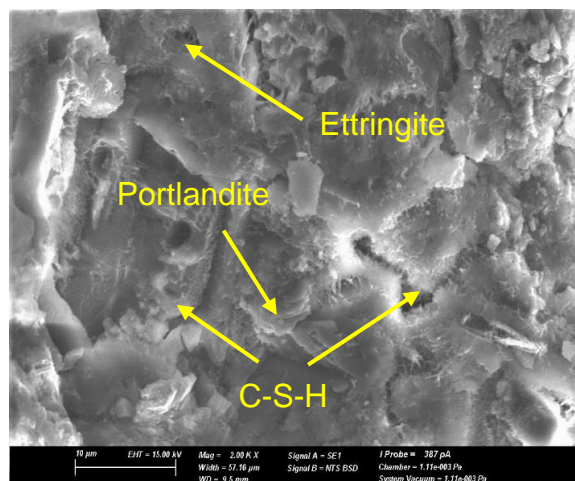
(d) OPC paste hydrated in S-water in 2 days

Fig. 11. Microstructure of OPC paste hydrated in D-water and S-water in 12 hr and 2 days

688

689

690

691

692
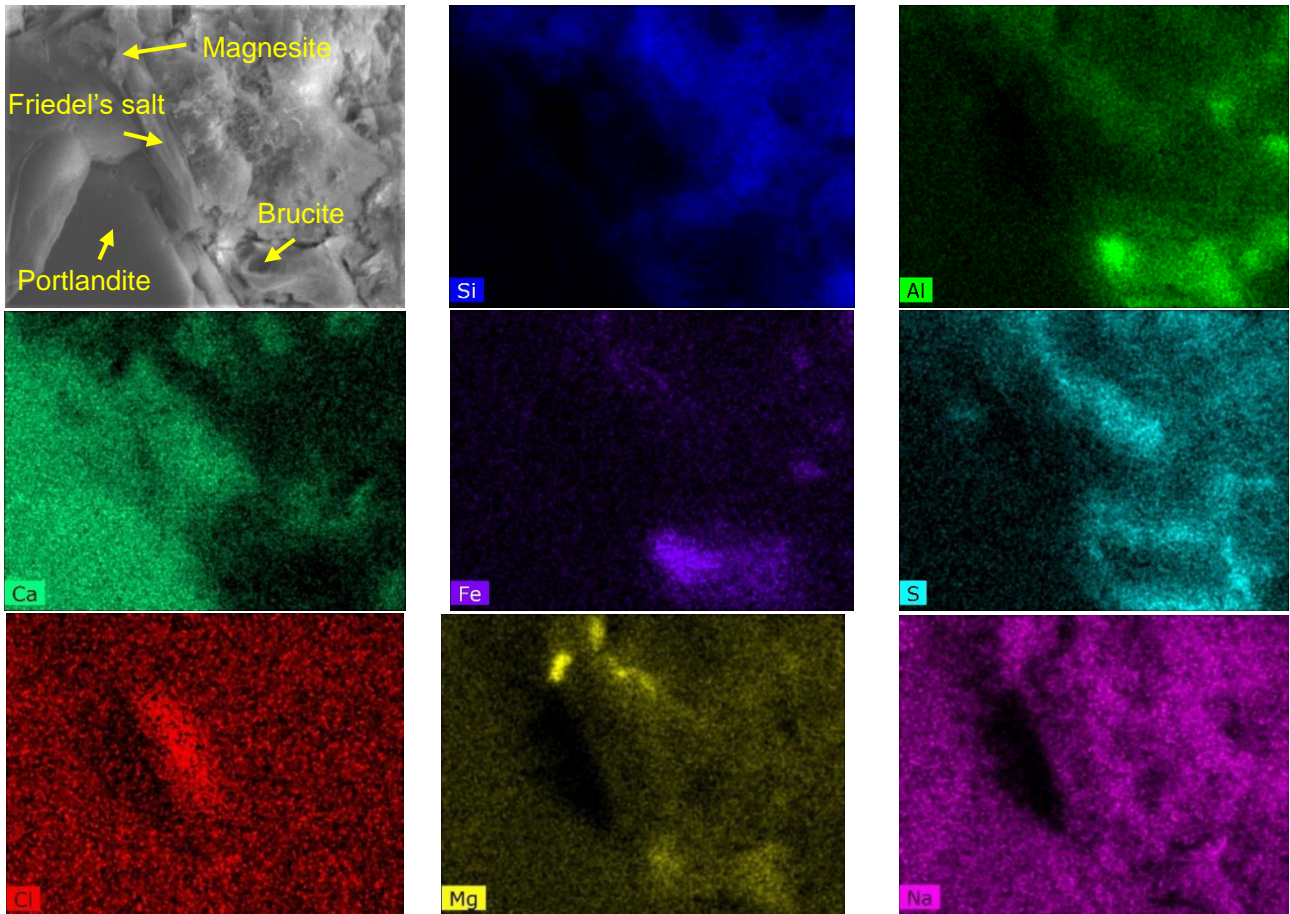
Fig. 12. Elemental mapping of microstructures of OPC paste hydrated in S-water for 4 days

693

694

695

696

697

698

699
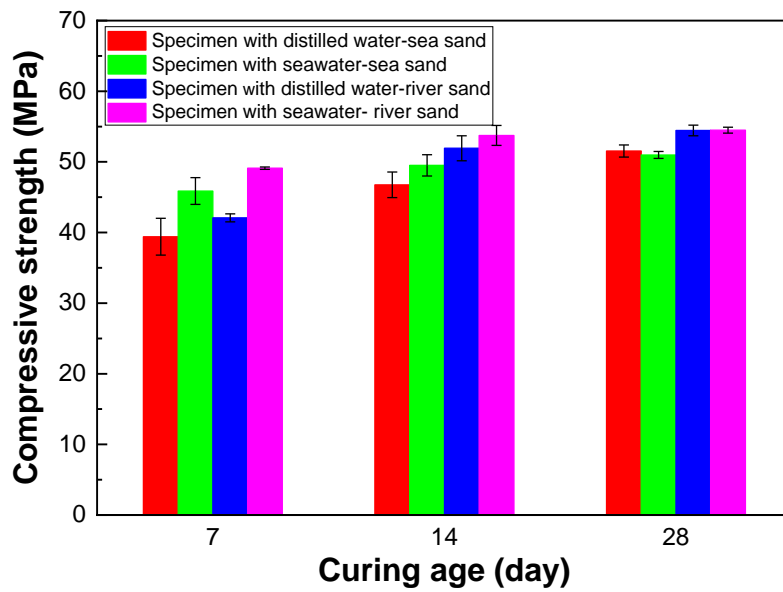
Fig. 13. Compressive strength of cement mortar with different types of water and sand
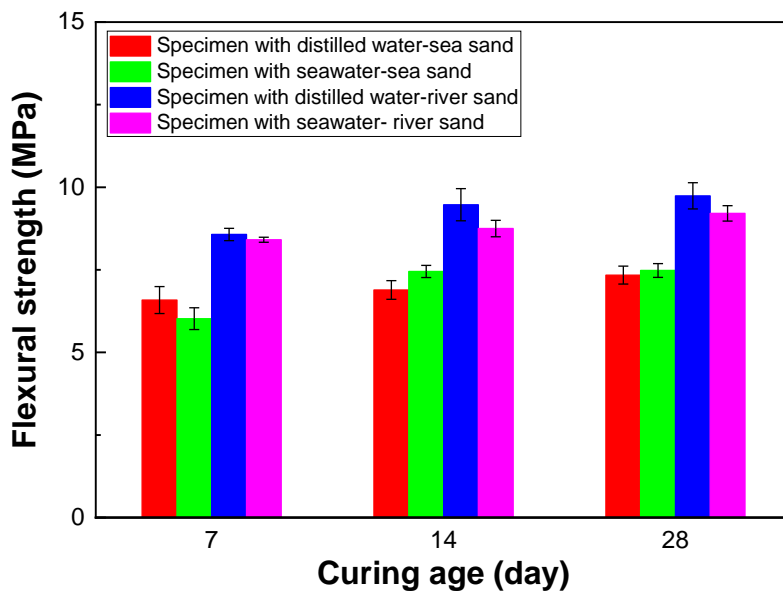
Fig. 14. Flexural strength of cement mortar with different types of water and sand

701

702